SUPPORTING INFORMATION

for

Functional identification of the first sodium binding site of the phosphate cotransporter NaPi-IIa (SLC34A1)

Cristina Fenollar-Ferrer[1†], Ian C Forster[2*†], Monica Patti[2], Thomas Knoepfel[2], Andreas Werner[3*‡], and Lucy R Forrest[1*‡]

[1]Computational Structural Biology Section,
Porter Neuroscience Research Center,
National Institutes of Neurological Disorders and Stroke,
National Institutes of Health,
Bethesda, MD 20892, USA

[2]Institute of Physiology and Zurich Center for Integrative Human Physiology,
University of Zurich,
Winterthurerstrasse 190,
CH-8057 Zürich
Switzerland

[3]Institute for Cell and Molecular Biosciences,
Epithelial Research Group
University of Newcastle upon Tyne,
Newcastle upon Tyne, NE2 4HH,
United Kingdom

Correspondence:
[*]lucy.forrest@nih.gov
[*]iforster@access.uzh.ch
[*]andreas.werner@newcastle.ac.uk

†Contributed equally as joint first authors.
‡Contributed equally as joint last authors.

Supporting Results

Activation indices for P_i and Na^+

The activation index was used to provide an initial indication of any significant change in the apparent substrate affinities of the mutants relative to the WT. Using a basic two point assay (e.g (1)), for P_i activation, we compare the electrogenic response with 0.1 mM P_i, close to the known WT $K_{0.5}^{Pi}$ (e.g. (2, 3)) with the response to 1 mM P_i that is close to saturating P_i for the WT. The index is given by the ratio $I_{Pi}^{0.1}/I_{Pi}^{1}$ determined at a defined membrane potential (–100 mV and with 100 mM Na^+ (100Na) as standard conditions). By assuming Michaelian kinetics, a non-linear relationship between $K_{0.5}^{Pi}$ and the index can be derived, based on the selected test concentrations (see Fig. S3A). Note that we consider the total P_i here. As P_i is titrated (at pH 7.4 the ratio $[HPO_4^{2-}]/[H_2PO_4^-] = 4:1$), the divalent P_i apparent affinity constant would be 20% smaller. For a ±30% change in $K_{0.5}^{Pi}$ (from the nominal 0.1 mM) that we consider within typical experimental variation for the WT, the P_i activation index would then vary from 0.49 to 0.63.

For Na^+ activation at saturating P_i (1 mM), the corresponding index is obtained by comparing the response to 1 mM P_i in 50 Na (close to the apparent $K_{0.5}^{Na}$ for the WT) with that in 100Na, i.e. ratio I_{Pi}^{50}/I_{Pi}^{100} (at –100 mV). We note that using the Na^+ activation index to detect changes in the apparent $K_{0.5}^{Na}$ is less certain because fits to the standard Na^+ activation data predict $K_{0.5}^{Na}$ and the Hill coefficient (n_H), a measure of cooperativity of Na^+ ion interactions, both of which might be influenced by the mutagenesis and thereby influence the index. Indeed, the Hill coefficient can vary considerably between isoforms (e.g., see (4)). The simulated curves (Fig. S3B) were generated for n_H = 2.0, 2.5 and 3.0 (the range experimentally reported for SLC34 proteins) and show how the corresponding apparent $K_{0.5}^{Na}$ varies, depending on the n_H chosen. For a ±30% change in $K_{0.5}^{Na}$ (from the nominal 50 mM) the Na^+ activation index would vary from 0.45 to 0.76 (assuming $n_H = 2.5$).

Dependence of the mid-point voltage ($V_{0.5}$) of presteady-state charge distribution on external **[Na^+]**

We consider a sequential 4–state model (states 0–3, Fig. 1), with transition 0↔1 representing the empty carrier and transitions 1↔2, 2↔3 representing the sequential binding of one Na^+ at each site (Na1, Na2). For the general case, if all partial reactions contribute to charge movement, the rate constants using Eyring rate theory (e.g., (5)), and assuming symmetrical barriers are given by:

$$
\begin{aligned}
k_{01} &= k_{01}^{0}\exp(-z_{01}Ve/2kT)\\
k_{10} &= k_{10}^{0}\exp(z_{01}Ve/2kT)\\
k_{12} &= [Na^{+}]k_{12}^{0}\exp(-z_{12}Ve/2kT)\\
k_{21} &= k_{21}\exp(z_{12}Ve/2kT)\\
k_{23} &= [Na^{+}]k_{23}^{0}\exp(-z_{23}Ve/2kT)\\
k_{32} &= k_{32}\exp(z_{32}Ve/2kT)
\end{aligned}
\qquad \text{S1a-f}
$$

where z_{01}, z_{12}, z_{23} are the valences of the equivalent charge that would be displaced across the whole membrane field associated with the respective partial reactions, k_{ij}^{0} is the rate for transition i→j for $V = 0$, [Na^+] is the Na^+ concentration, and e, k, T have their usual meanings.

The charge displaced by a voltage step from $V = +\infty$ (i.e. N_t transporters in state 0) to a potential V, can be expressed as (see (6)):

$$
Q_{\infty}^{V} = -N_t e\left[\frac{\left((z_{01}+z_{12}+z_{23})+(z_{12}+z_{23})\alpha+z_{23}\alpha\beta\right)}{1+\alpha+\alpha\beta+\alpha\beta\gamma}\right] \qquad \text{S2}
$$

where $\alpha = k_{01}/k_{10}$, $\beta = k_{12}/k_{21}$ and $\gamma = k_{23}/k_{32}$. The voltage at which 50% of the total charge has moved ($V_{0.5}$) is found by solving Eq. S2 for V and setting $Q = 0.5N_t e$ (z_{01}+z_{12}+z_{23}), to give the implicit function:

$$
(z_{01}+z_{12}+z_{23})(1-0.5(1+\alpha+\alpha\beta+\alpha\beta\gamma))+\alpha(z_{12}+z_{23})+\alpha\beta z_{23} = 0 \qquad \text{S3}
$$

Note, that in the limit, for [Na^+] large, Eq. S3 simplifies to:

$$
\alpha^{0}\beta^{0}\gamma^{0}\left[Na^{+}\right]^{2}(e^{-eV_{0.5}(z_{01}+z_{12}+z_{23})/kT}) = 1 \qquad \text{S4}
$$

where $\alpha^0 = k^0_{01}/k^0_{10}$, $\beta^0 = k^0_{12}/k^0_{21}$ and $\gamma^0 = k^0_{23}/k^0_{32}$ and this yields an explicit solution for $V_{0.5}$. For one net charge translocated across the transmembrane field, the predicted slope of the $V_{0.5}$ vs $\log_{10}$[Na^+] relation is then 116mV/decade at 20 ºC.

The $V_{0.5}$ vs [Na^+] data set with non-zero [Na^+] (Fig. 6B) were fit using the Curve Fitting Toolbox in Matlab 2014b (Fig. 6C). We used the mean value of $V_{0.5}$ with 0Na and assumed $z_{01} = 0.7$ to predict α^0, which was then fixed, and z_{01}+z_{12}+$z_{23} = 1$, where $z_{23} = 0$. The unknown parameters β^0, γ^0 were estimated using a trust-region algorithm. The fit parameters and RMSE are given in Table S3.

Supporting Tables

Table S1: Cα-Cα distances and Cα-Cα-Cβ angles between pairs of residues close to Na1 in models of human NaPi-IIa in which the alignment of L2ab-TM2b has been adjusted

	Distance (Å)		Angle (°)		
Model	227-206	227-209	227-206	227-209	227-210
Initial[a]	10.6	13.5	109	169	61
1	12.1	10.4	158	73	48
2	10.4	6.3	83	36	128
3	13.5	11.5	162	132	97
4	9.8	12.5	67	100	15
5	6.4	9.4	38	27	82

[a]Values for the initial, published model (7).

Table S2: Cα-Cα distances and Cα-Cα-Cβ angles between pairs of residues in models of human NaPi-IIa in which the alignment of TM5a-L5ab has been adjusted

	Distance (Å)		Angle (°)	
Model	419-451	447-206	419-451	447-206
5	9.8	7.2	108	114
6	8.8	9.7	106	164
7	5.4	8.8	52	95
8	6.4	5.1	103	29

Table S3: Fit parameters for fit of Eq. S3 to mean $V_{0.5}$ *vs* $\log_{10}[Na^+]$ data

Construct	α^0	β^0	γ^0	*RMSE*
WT	0.14	7.41	12.24	0.0457
D209A	0.20	0.38	39.85	0.0123
D209E	0.20	0.16	64.5	0.0405
R210A	0.10	1.084	110	0.0876
S447A	0.12	0.081	773	0.0494

Table S4. Summary of Boltzmann fit parameters for individual oocytes in Fig. 5A

Construct	Superfusate	Q_{hyp} (nC)	Q_{max} (nC)	z	$V_{0.5}$ (mV)
WT	0Na	–1.73 ± 0.07	3.65 ± 0.11	0.63 ± 0.03	–54 ± 2
	100Na	–1.29 ± 0.08	4.35 ± 0.19	0.71 ± 0.06	–27 ± 3
D209E	0Na	–5.37 ± 0.50	8.18 ± 0.67	0.31 ± 0.03	–112 ± 8
	100Na	–1.29 ± 0.08	9.27 ± 0.08	0.47 ± 0.10	–77 ± 1
T454A	0Na	–2.40 ± 0.11	3.77 ± 0.14	0.50 ± 0.03	–86 ± 3
	100Na	–2.02 ± 0.14	3.24 ± 0.19	0.66 ± 0.07	–75 ± 4

Supporting Figures

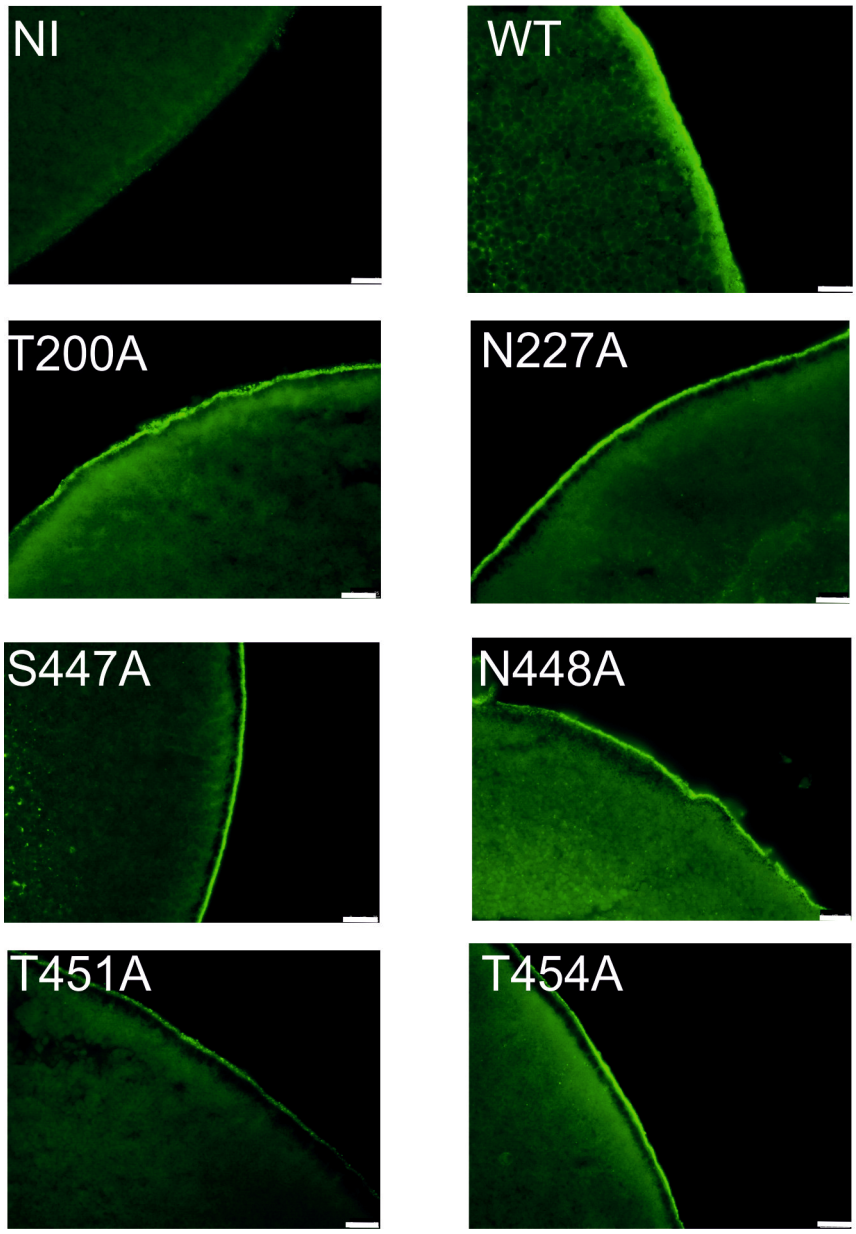

Figure S1: Immunocytochemical evidence for membrane expression of non-functional mutants. Immunocytochemistry of constructs identified as non-functional (see Table 1, (7)) confirmed that the corresponding protein was present in the oocyte membrane. Images shown for representative non-injected oocyte (NI), wild-type human NaPi-IIa (WT) and mutants: T200A, N227A, N447A, T448A, T451A, and T454A (see Text for details). Scale bar = 50 μm.

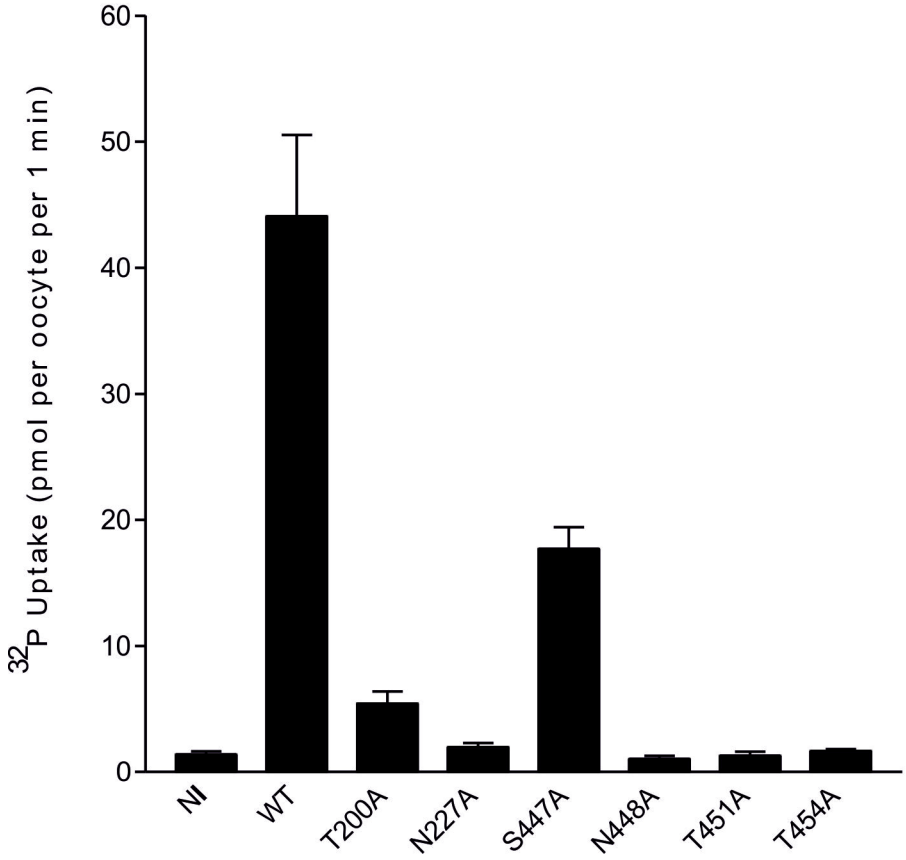

Figure S2: $^{32}P_i$ uptake assay performed on selected constructs.

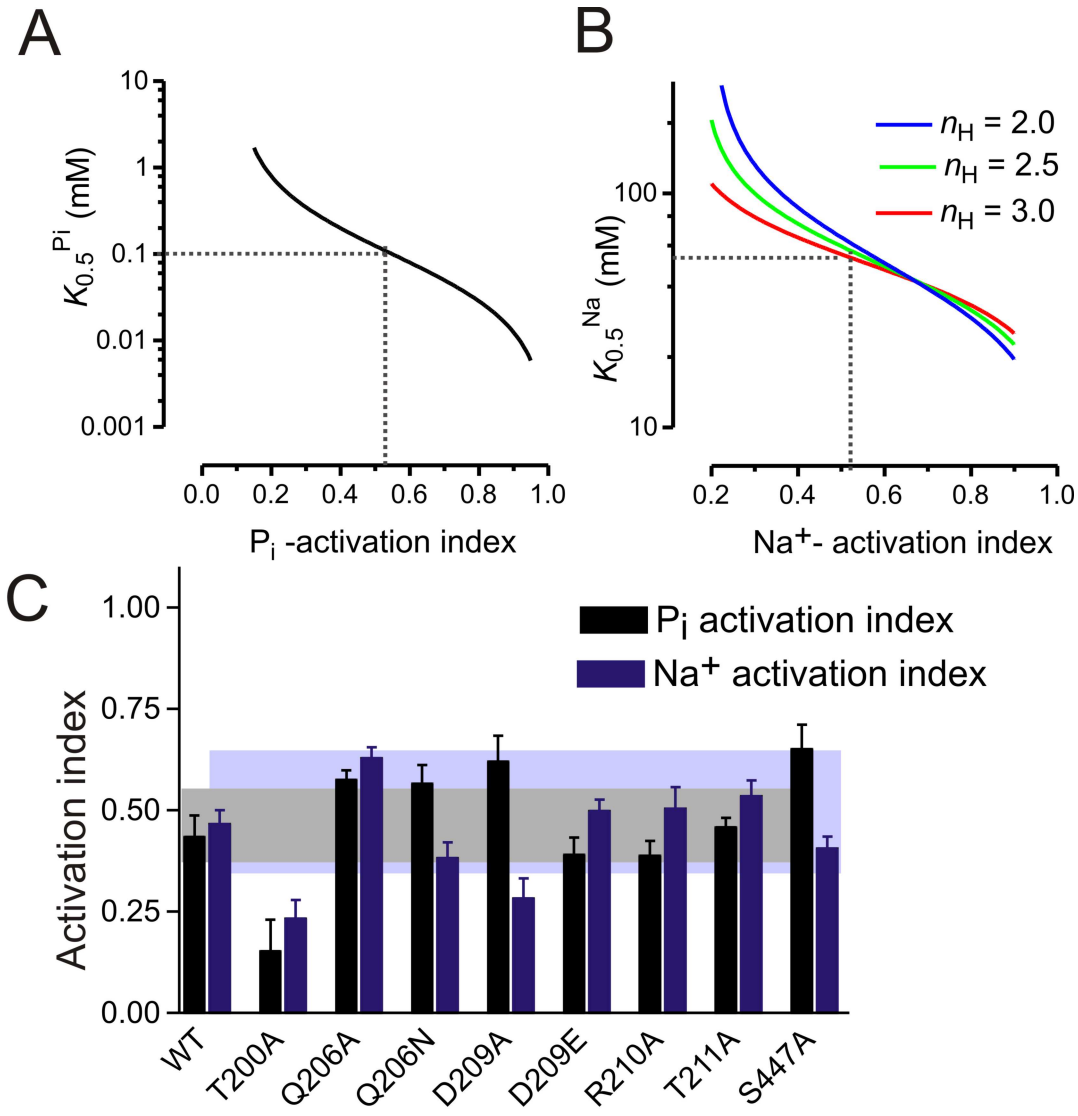

Figure S3: **Activation indices**. (*A, B*) Relationship between $K_{0.5}^{Pi}$ and activation indices – see Supporting Results for details. (*C*) Summary of the P_i and Na^+ activation indices for all mutants that gave a resolvable I_{Pi}. P_i (*black bars*) and Na^+ (*blue bars*) activation indices for WT human NaPi-IIa and mutants with substitutions in RU1 as indicated, at –100 mV. Each black bar represents $I_{Pi}^{0.1}/I_{Pi}^{1}$ as defined above (P_i activation index). Each blue bar represents I_{Pi}^{50}/I_{Pi}^{100} as defined above (Na^+ activation index). All data shown as mean ± sem for $n > 10$ oocytes from several donor frogs. The grey box represents the predicted range of the P_i-activation index if the P_i apparent affinity constant ($K_{0.5}^{Pi}$) were to change by ±30% with respect to the WT value. Similarly, for Na^+-activation, the light blue box represents the expected range of the Na^+-activation index if the apparent Na^+-affinity constant ($K_{0.5}^{Na}$) were to change by ±30% with respect to the WT value.

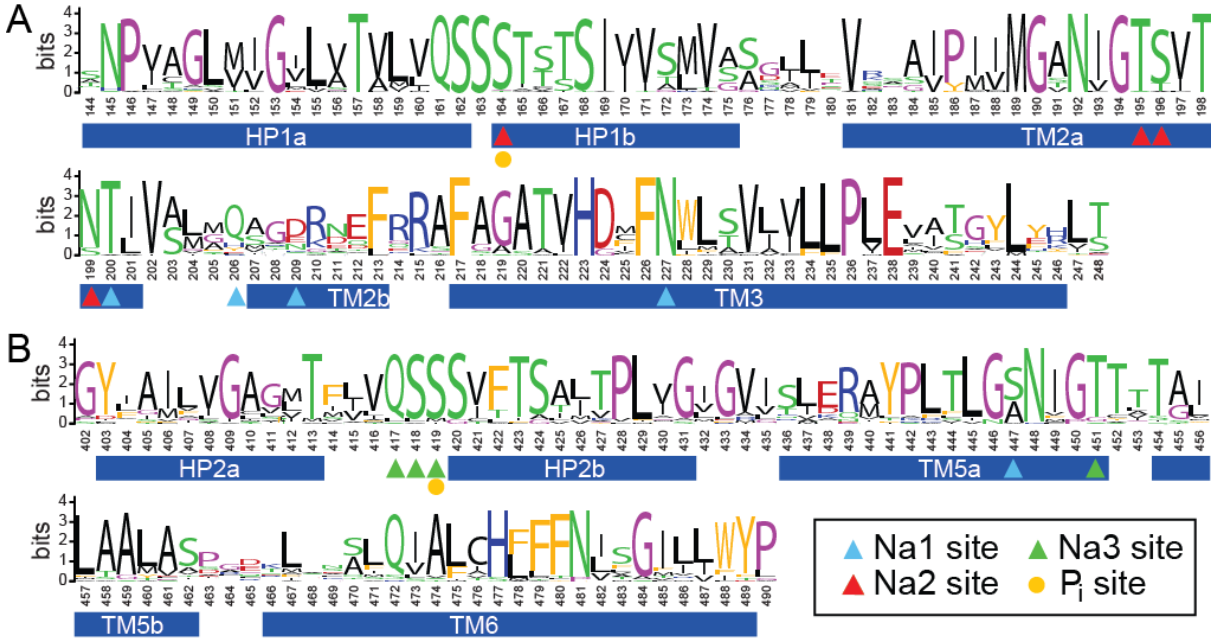

Figure S4: **Sequence logo illustrating the conservation of residues (*A*) 144-248 in repeat 1 and (*B*) 402-490 in repeat 2.** The TM helices in the model are indicated by blue rectangles. Residues predicted to be involved in P_i, Na1, Na2 and Na3 binding are indicated with yellow circles, and blue, red, and green triangles, respectively. The input multiple sequence alignment comprised 50 sequences obtained by HHblits (8) from a search of the nr20 NCBI database (see Methods). The logo was generated using the Weblogo3 webserver (9). The residues are colored as follows: aromatic (W, Y, F) in orange, polar (S, T, N, Q) in green, basic (R, K, H) in blue, hydrophobic (V, A, L, I, M) in black, acidic (E, D) in red, and P and G in magenta.

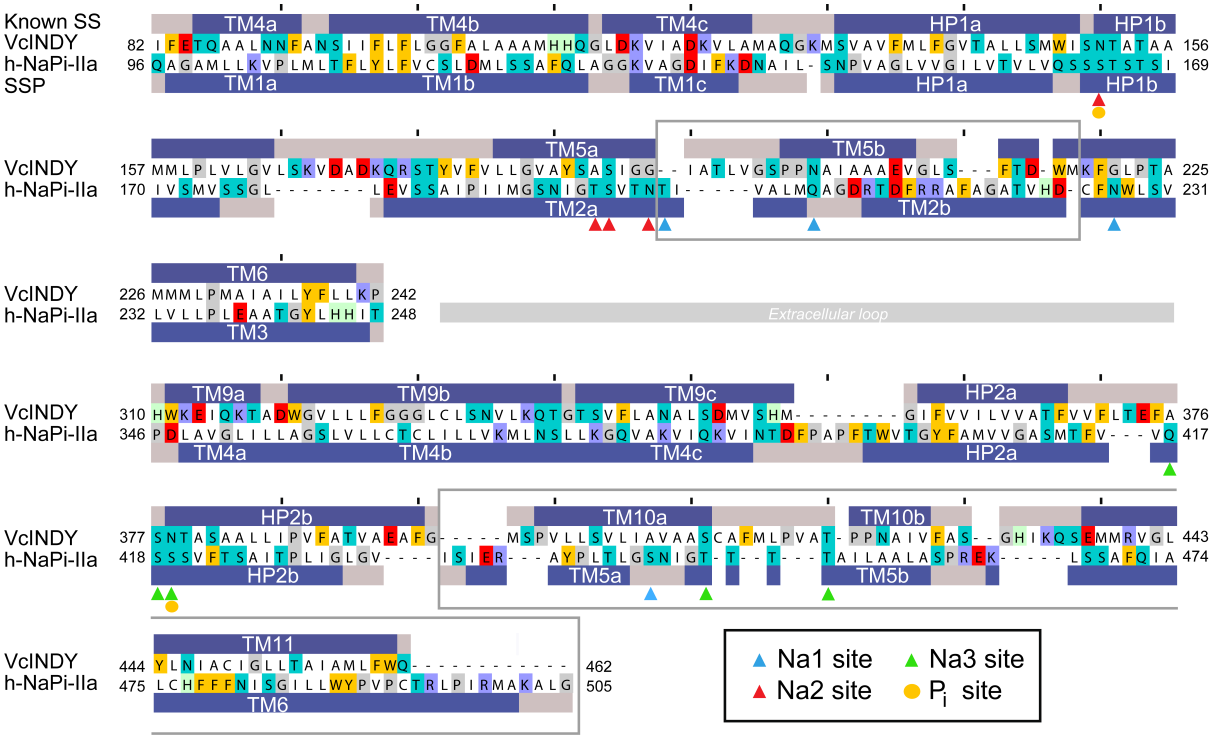

Figure S5. Sequence alignment between the core region of human-NaPi-IIa and the template VcINDY used for the modeling of the refined model. Segments that have been adjusted during the refinement are marked with open grey boxes. The helices assigned from the structure of VcINDY (labeled "Known SS") and the PSIPRED v3.2 (10) secondary structure predictions for helices in NaPi-IIa (labeled "SSP") are shown as blue bars above and below the sequences, respectively. Residues whose side chains contribute to the P_i, Na1, Na2 or Na3 sites are indicated with yellow spheres, and blue, red and green triangles, respectively.

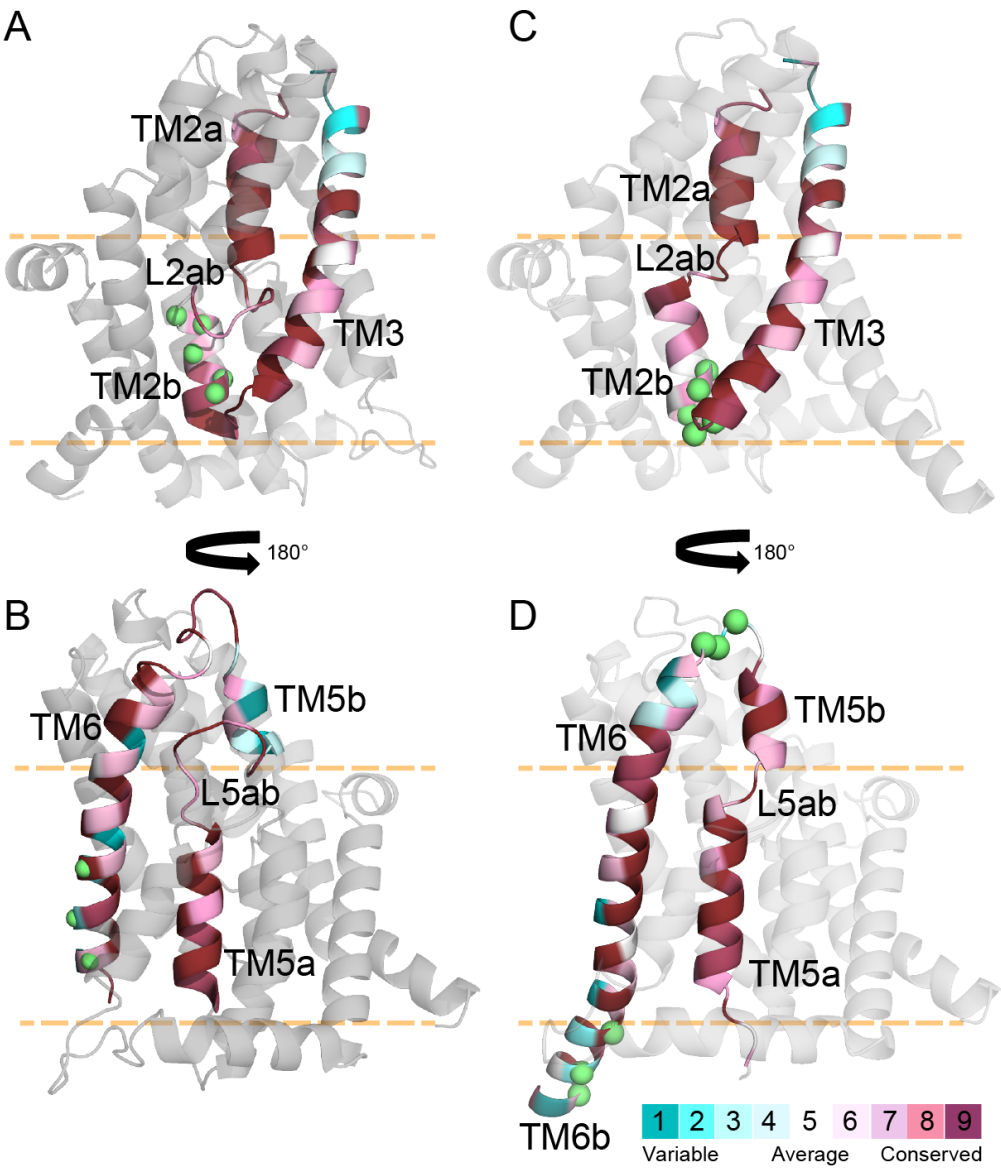

Figure S6. **Evolutionary conservation analysis of human NaPi-IIa models**. ConSurf (11) profiles are mapped onto models of human NaPi-IIa, before (*A, C*) and after (*B, D*) adjustment of the target-template sequence alignment in the TM2-3 (*A, B*) and TM5-6 (*C, D*) regions. The protein is viewed from along the plane of the membrane, with the cytoplasm toward the bottom; the approximate extents of the hydrophobic core of the membrane are indicated by orange dashed lines. The position of charged residues whose locations are less buried in the refined model, are indicated by green spheres for the Cα atoms. In the refined model, more evolutionarily conserved residues (*dark pink*) face towards the core of the protein, while more variable residues (*cyan*) face away from the protein core.

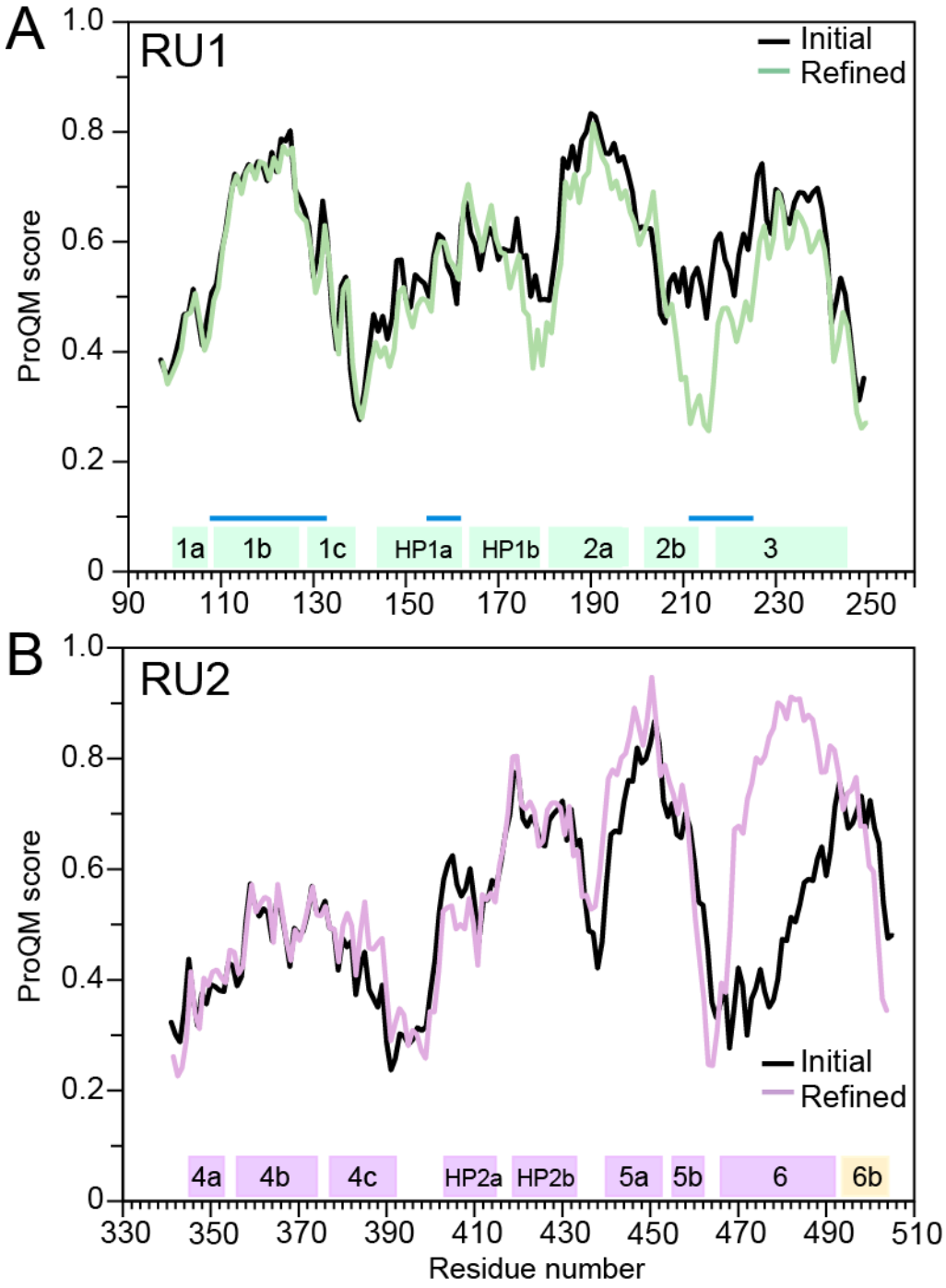

Figure S7. Protein quality score per residue, measured using ProQM for the initial and refined models of NaPi-IIa, and window-averaged along the sequence. Scores for the initial model are shown in black, while the ProQM scores of (*A*) repeat unit 1 and (*B*) repeat unit 2, are shown in green and pink, respectively. The extents of the helical segments in the refined model are shown underneath the scores, and labeled according to their position in the structure. Segments whose template equivalents are in contact with peripheral helices are indicated using blue bars.

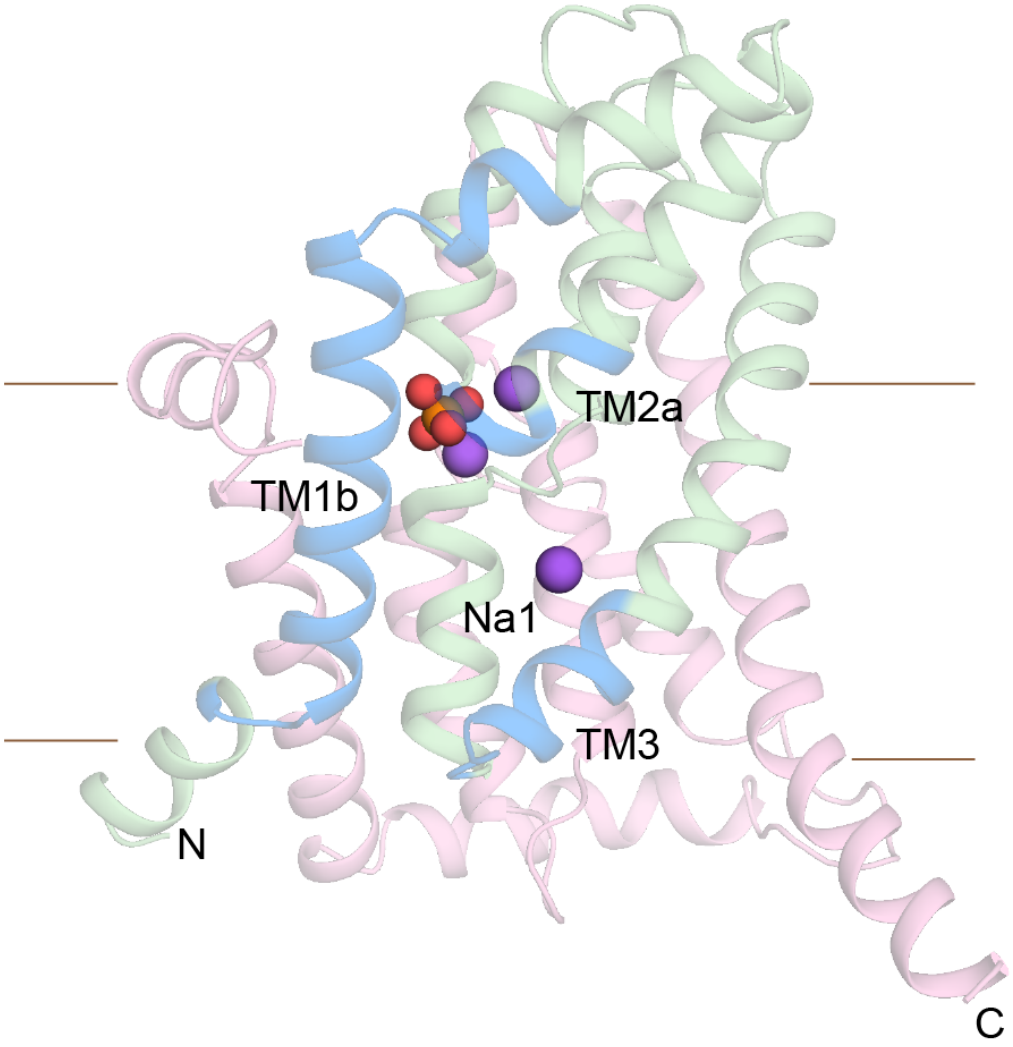

Figure S8. Model of human-NaPi-IIa indicating the position of segments involved with helix contacts in the template structure. The crystal structure of VcINDY was structurally superimposed on the model NaPi-IIa using PyMOL (Version 1.7.0.5, Schrödinger, LLC); any residues of NaPi-IIa within 8 Å of the peripheral helices TM7-8 in VcINDY have been highlighted in blue. The protein is viewed from within the plane of the membrane with the cytoplasm toward the bottom. The approximate extents of the membrane are indicated using brown lines. Repeats 1 and 2 are colored green and pink, respectively. Na^+ ions and P_i substrate are shown as spheres.

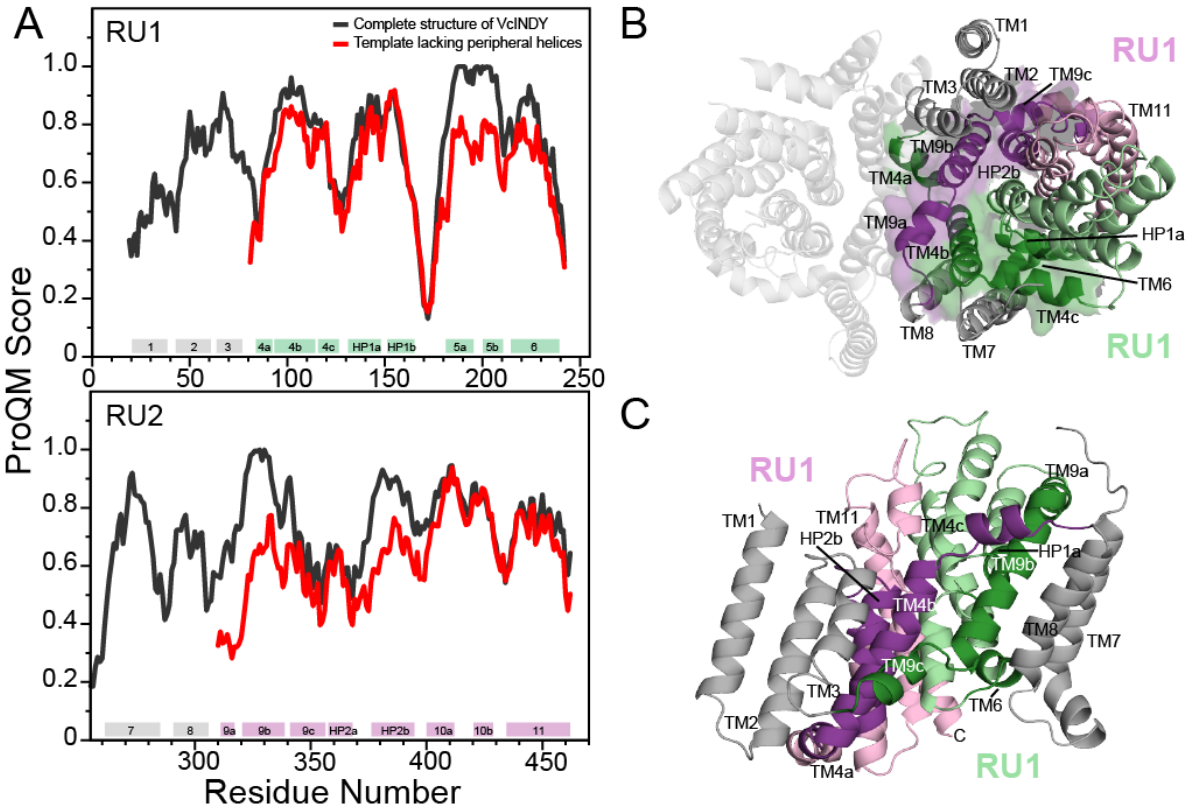

Figure S9. Comparison of ProQM scores for full-length structure of VcINDY and the template used in the NaPi-IIa modeling, after deleting several peripheral segments. (*A*) ProQM score (12) per residue for repeats 1 (*top panel*) and 2 (*bottom panel*) for VcINDY structure (*black line*) and template used (*red line*). The total ProQM scores are 0.675 for the VcINDY structure, and 0.643 for the truncated template used. TM domains not used during the modeling are highlighted using grey rectangles, while those used for modeling repeats 1 and 2 are indicated using green and pink rectangles, respectively. (*B*) Cytoplasmic view, and (*C*) view of dimerization interface for the X-ray structure of VcINDY dimer shown in cartoon for protomer A and Cα-trace for protomer B. Peripheral helices TM1-3 and 7-8 are colored grey, repeats 1 and 2 in green and pink respectively. Residues within 8 Å of TM1-3 and/or TM7-8 are highlighted in dark green in repeat 1 or purple in repeat 2.

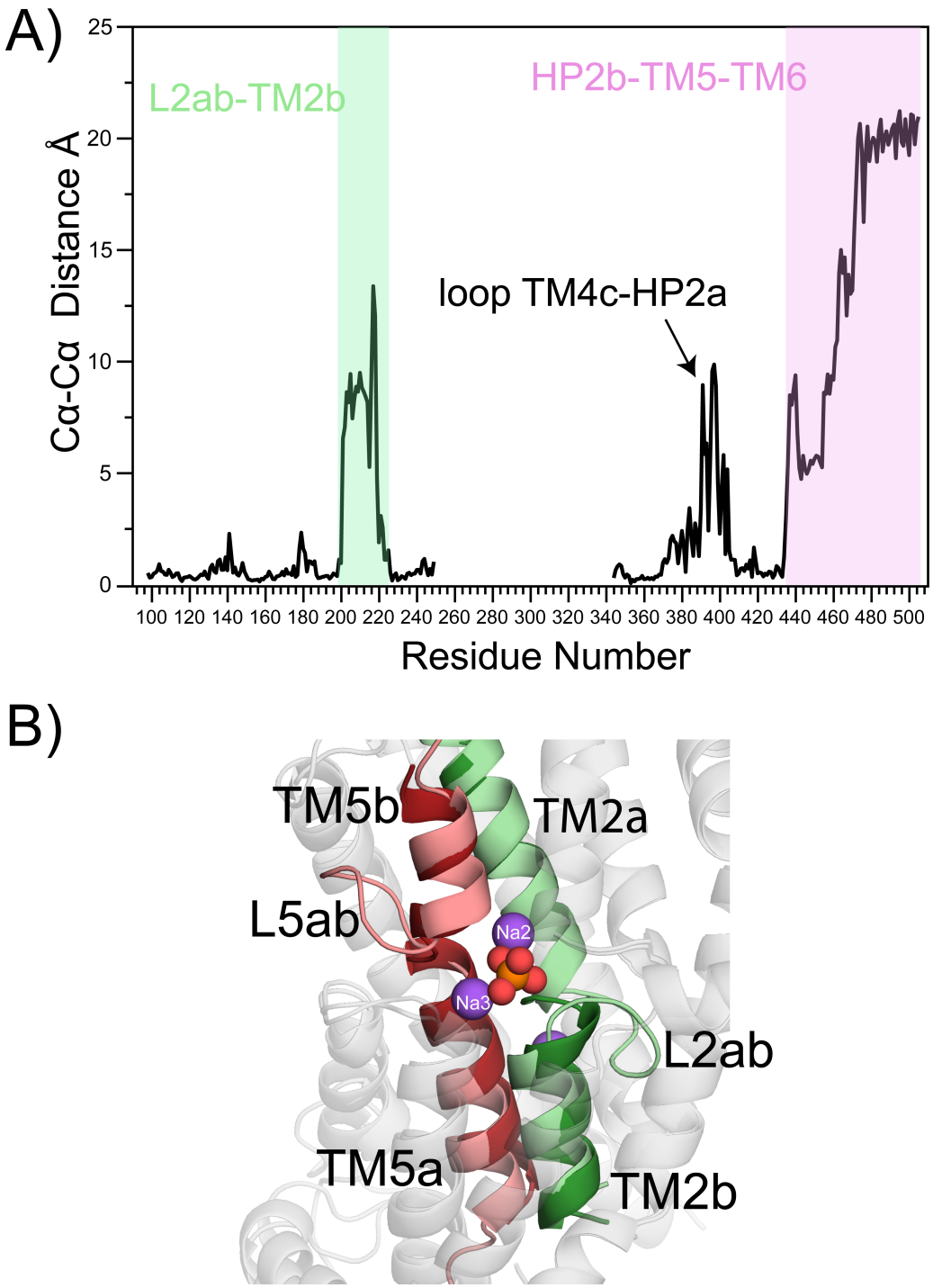

Figure S10. Comparison of the hNaPi-IIa model presented in this work and the previous model published by Fenollar-Ferrer et al. (7). (*A*) Cα-Cα distance for each residue between the two models after structural superposition. The segments that change the most between models, as a consequence of the new alignment and constraints, are highlighted in green and pink for RU1 and RU2 respectively. (*B*) Comparison of the L2ab and L5ab loops in the two models after structural superposition. TM5 is shown in red and pink (new and previous model, respectively), while TM2 is shown in green and pale green (new and previous model, respectively).

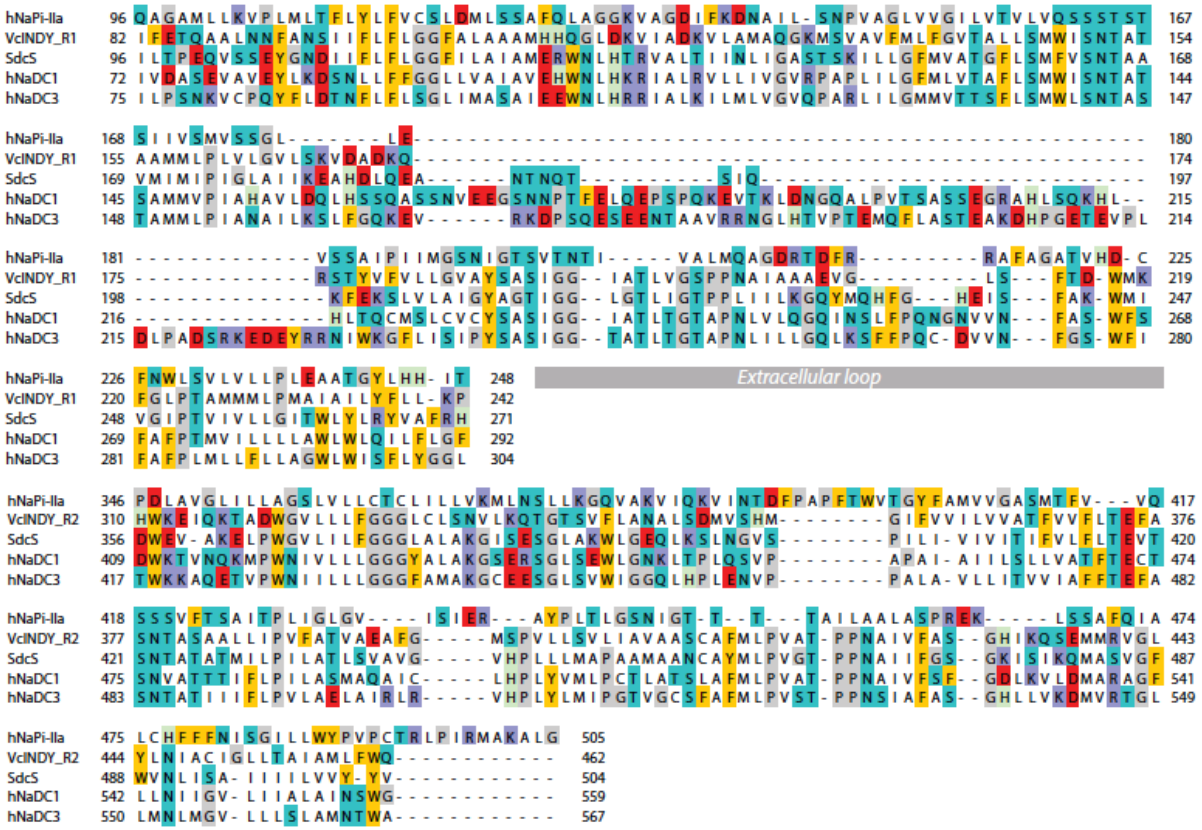

Figure S11. Sequence alignment between the core region of human-NaPi-IIa, the template VcINDY, and homologs of VcINDY including: SdcS from *Staphylococcus aureus*, and the SLC13 family members human NaDC1 and human NaDC3. The sequence alignment between VcINDY and its homologs was constructed using MSAProbs (13).

Supporting References

1. Ehnes, C., I. C. Forster, K. Kohler, A. Bacconi, G. Stange, J. Biber, and H. Murer. 2004. Structure-function relations of the first and fourth predicted extracellular linkers of the type IIa Na^+/Pi cotransporter: I. Cysteine scanning mutagenesis. *J. Gen. Physiol*. 124:475-488.
2. Virkki, L. V., I. C. Forster, J. Biber, and H. Murer. 2005. Substrate interactions in the human type IIa sodium-phosphate cotransporter (NaPi-IIa). *Am. J. Physiol.* 288:F969-F981.
3. Virkki, L. V., I. C. Forster, N. Hernando, J. Biber, and H. Murer. 2003. Functional characterization of two naturally occurring mutations in the human sodium-phosphate cotransporter type IIa. *J. Bone Miner. Res.* 18:2135-2141.
4. Forster, I. C., D. D. Loo, and S. Eskandari. 1999. Stoichiometry and Na^+ binding cooperativity of rat and flounder renal type II Na^+-P_i cotransporters. *Am. J. Physiol.* 276:F644-649.
5. Hille, B. 2001. Ion channels of excitable membranes. Sinauer, Sunderland, Mass.
6. Andrini, O., A. K. Meinild, C. Ghezzi, H. Murer, and I. C. Forster. 2012. Lithium interactions with Na^+-coupled inorganic phosphate cotransporters: insights into the mechanism of sequential cation binding. *Am. J. Physiol. Cell. Physiol.* 302:C539-554.
7. Fenollar-Ferrer, C., M. Patti, T. Knopfel, A. Werner, I. C. Forster, and L. R. Forrest. 2014. Structural fold and binding sites of the human Na(+)-phosphate cotransporter NaPi-II. *Biophys. J.* 106:1268-1279.
8. Remmert, M., A. Biegert, A. Hauser, and J. Soding. 2011. HHblits: lightning-fast iterative protein sequence searching by HMM-HMM alignment. *Nat. Methods* 9:173-175.
9. Crooks, G. E., G. Hon, J. M. Chandonia, and S. E. Brenner. 2004. WebLogo: a sequence logo generator. *Genome Res*. 14:1188-1190.
10. Jones, D. T. 1999. Protein secondary structure prediction based on position-specific scoring matrices. *J. Mol. Biol.* 292:195-202.
11. Ashkenazy, H., E. Erez, E. Martz, T. Pupko, and N. Ben-Tal. 2010. ConSurf 2010: calculating evolutionary conservation in sequence and structure of proteins and nucleic acids. *Nucleic Acids Res* 38:W529-533.
12. Ray, A., E. Lindahl, and B. Wallner. 2010. Model quality assessment for membrane proteins. *Bioinformatics* 26:3067-3074.
13. Liu, Y., B. Schmidt, and D. L. Maskell. 2010. MSAProbs: multiple sequence alignment based on pair hidden Markov models and partition function posterior probabilities. *Bioinformatics* 26:1958-1964.